T1.5-P16

SEISMOTECTONIC IMPLICATIONS OF THE 20 MAY 1990 SOUTH SUDAN EARTHQUAKE

Josphat K. Mulwa[1] and Fumiaki Kimata[2]

[1]University of Nairobi, Department of Geology, P.O. Box 30197-00100, Nairobi, Kenya; E-mail: Josphat_mulwa@yahoo.com; jkmulwa@uonbi.ac.ke

[2]Tono Research Institute of Earthquake Science, Association for the Development of Earthquake Prediction, 1-63 Akiyo, Mizunami, 509-6132, Gifu, Japan; E-Mail: fumikimata@gmail.com

Introduction:

The south Sudan earthquake of May 20, 1990 is so far among the three strongest ($M_w \geq 7.0$) earthquakes to occur in the eastern part of Africa since 1910. This earthquake caused damage in south Sudan as well as severe shaking in parts of Uganda and Kenya, and was accompanied by two strong aftershocks on May 24, 1990 (M_w = 6.5 and 7.1).

Methodology:

Teleseismic body wave inversion has been applied to determine source parameters and the implications of the May 20, 1990 south Sudan earthquake on the seismotectonics of south Sudan and the central and southeastern parts of Kenya. Digital broadband seismic waveform data was extracted from Global Seismographic Network (GSN) of Incorporated Research Institutions for Seismology (IRIS) webpage for both II and IU networks. In order to improve the results and final solution, additional broadband seismic waveform data was obtained from the IRIS webpage for various other seismic networks such as China Digital Seismograph Network (CD), Digital Standardized Seismographic Network (DW), GEOSCOPE (G), German Regional Seismic Network (GR), and MEDNET Project (MN).

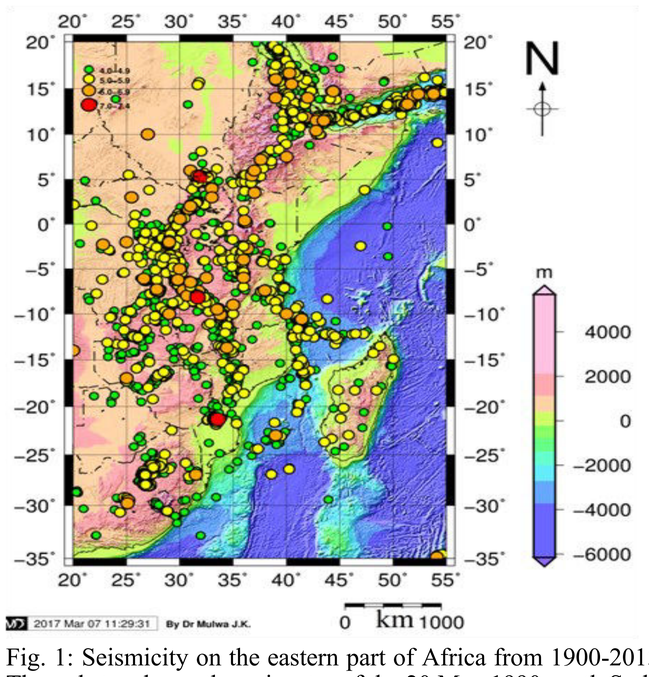

Fig. 1: Seismicity on the eastern part of Africa from 1900-2015 for $M_w \geq 4.0$. The red star shows the epicentre of the 20 May 1990 south Sudan earthquake

Twenty three (23) seismograms from nineteen (19) seismic stations characterized by good signal-to-noise ratio were selected. The source-seismic stations distance range was limited to 30° - 100°. Distance range is appropriate so as to make use of stable seismic rays travelling mostly in the lower mantle which are free of complexities caused by reflection or refraction in the upper mantle and near the core-mantle boundary (Yoshimoto and Ando, pers comm.). P-wave seismograms consist of the direct P wave and the depth phases, $_pP$ and $_sP$. The horizontal P-wave seismograms were rotated to generate transverse (SH) components (Kikuchi and Kanamori, 1991). The P- and SH– waveforms were equally sampled at 10-20 Hz and synthetic seismograms for P- and SH- components generated by summation of normal modes at periods of 80 seconds for both synthetic and observed seismograms (Kikuchi and Kanamori, 1991). Observed and synthetic P- and SH- seismograms were band-pass filtered between 0.02 Hz and 1 Hz. This frequency band provides a convenient characterization of the rupture process for teleseismic source spectrum (Houston, 1990). A weighting scheme for the synthetic and observed seismograms was introduced and time correction computed for each observed seismograms so as to match their P- and SH- phase onset times with that of the synthetic seismograms. Inversion of P- and SH- waveforms was then undertaken as discussed by Kikuchi and Kanamori (1991); Kikuchi et al., (1993) and, Thio and Kanamori (1996).

The first step of waveform inversion was computation of theoretical Green's function using the generalized ray method (Helmberger, 1983) and the global average earth velocity model of IASPEI91 (Kennett and Engdahl, 1991). The focal depth (14.9 km) by USGS/ NEIC was used for the starting model, and theoretical Green's function was then computed during inversion by variance minimization using a trial and error approach. For this first step of the inversion, the best result was obtained by using eleven (11) discrete depths at intervals of 2.8 km. This ensured that the focal depth was varied from a shallow 0.9 km to 28.9 km, hence covering almost the entire crust. During the inversion, the fault plane was represented by nodal points equally spaced at 40 km in the strike direction.

Earthquake source-time function was obtained by deconvolving the vertical component of teleseismic P-waveforms with the impulse response (source-free) synthetic seismograms. The source-time function was parameterized into a sequence of two overlapping isosceles triangular elements having a total base length of 13.2 seconds and time increments of 6.6 seconds. Inversion of the seismograms to retrieve initial fault mechanism, seismic moment, moment magnitude, strike, dip, rake, rupture start time, location of rupture front, as well as variance in focal depth was then undertaken by minimizing the misfit, in a least squares sense, between observed and synthetic seismograms.

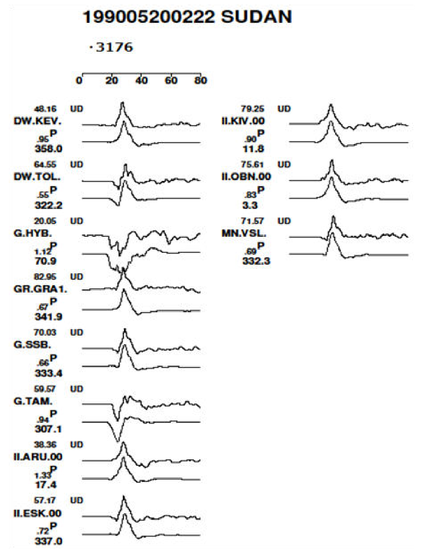

Fig. 3a: Results of P- waveforms inversion. The upper and lower waveforms are observed and synthetic seismograms respectively.

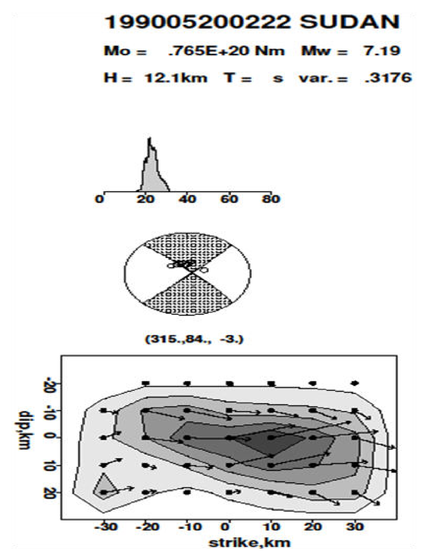

Fig. 3b: Source-time function, focal mechanism and fault rupture pattern obtained from robust inversion of P-waves

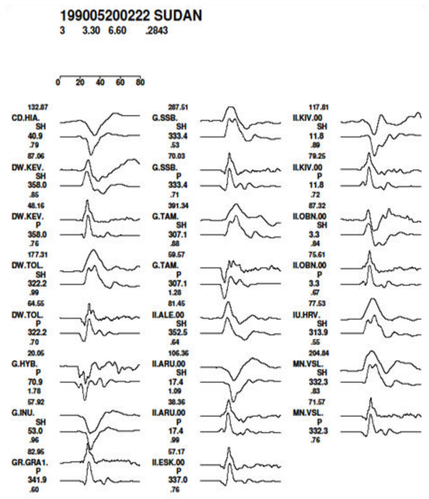

Fig. 2a: P- and SH- waveforms inverted as discussed in the preceding section to obtain the solution in figure 2b. The upper and lower waveforms are observed and synthetic seismograms respectively.

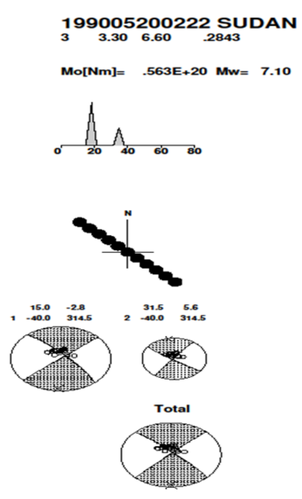

Figure 2b: Source time function, fault plane and focal mechanism obtained from inversion of P- and SH- waveforms.

A robust second step of teleseismic body wave inversion involved only P- waveforms. The earthquake source parameters were modeled as point double-couple with a time dependent source time function parameterized into a sequence of six overlapping isosceles triangular elements each having a base length of two seconds, and time increments of one second. Other variable parameters incorporated in this stage of inversion were strike, dip, rake, focal depth and rupture start time as obtained from the first step of the waveforms inversion. Additional parameters included rupture front velocity (V_r) and the fault plane represented by a grid scheme in kilometers in x- and y- directions.

Results:

Figures 3a and 3b show the final results of the robust inversion obtained by inverting only the P-waveforms as discussed in the preceding section.

The results of teleseismic body wave inversion show that the best solution consists of only one event with a source mechanism of 315°/84°/-3° (strike/dip/rake). The focal mechanism is predominantly strike-slip and the fault rupture pattern (figure 3b) demonstrates that the strike-slip fault mechanism is left-lateral. The focal depth for this earthquake is 12.1 km, seismic moment M_o = 7.65 x 10^{19} Nm and moment magnitude, M_w = 7.19 (≅7.2). The fault rupture started 15 seconds earlier and lasted for a duration of 17 seconds along a fault plane having dimensions of length 60 km and width 40 km, as deduced from the source-time function and rupture pattern respectively. An average dislocation of 1.1 m was obtained from the inversion results and the calculated stress drop (σ), based on equation by Fukao and Kikuchi (1987), is 1.63 Mpa.

Conclusions:

Figure 4 shows NW-SE trending rift/shear zones as well as some strong historical earthquakes in the East Africa region. The left-lateral strike-slip fault mechanism due to the south Sudan earthqauke is consistent with that of the January 6, 1928 (M_s = 6.9) Subukia earthquake in central Kenya. Further, the distribution of strong earthquakes from south Sudan through central Kenya shows a NW-SE alignment of epicenters. On a local scale in Kenya, the NW-SE alignment of epicenters is characterized by earthquakes of local magnitude $M_l \leq 4.0$, except the January 6, 1928 Subukia earthquake. This NW-SE alignment of epicenters supports a strong inference for a NW-SE extension of a transform fault zone from southern Sudan through central Kenya and further SE into the Indian Ocean, which is consistent with the trend of Aswa-Nyangia transform fault zone.

The results of this study demonstrate that, the May 20, 1990 south Sudan earthquake is not due to extension and normal faulting of the western branch of the East African Rift System but rather due to re-activation and subsequent strike–slip fault motion of the NW-SE trending Aswa fault (shear) zone which extends into Kenya as Aswa-Nyangia fault zone (ANFZ).

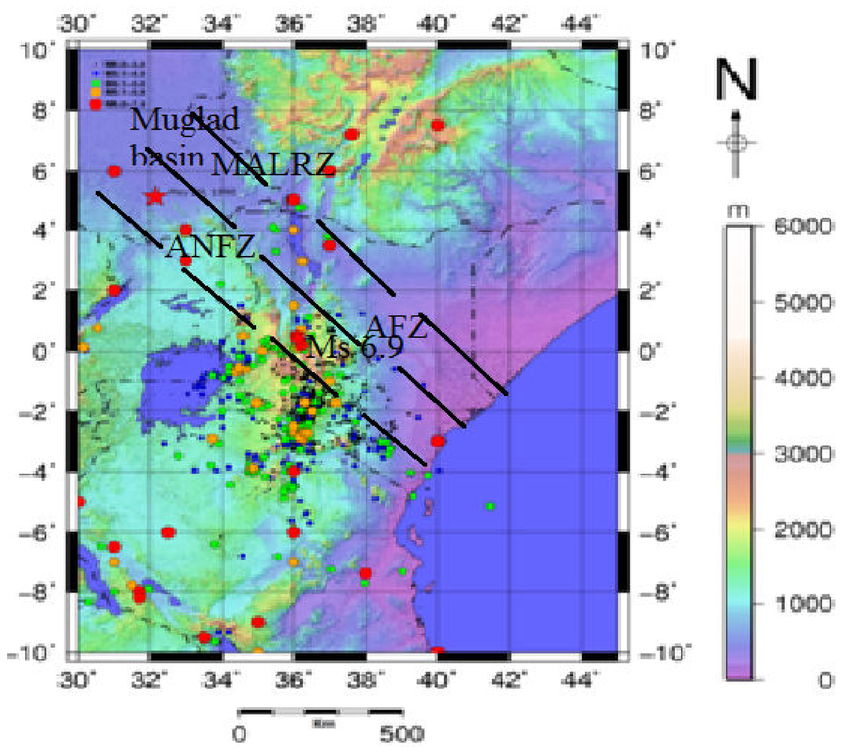

Fig. 4: NW-SE alignment of tectonic structures and epicenters of some historical earthqaukes in the East Africa region. MALRZ = Muglad-Anza-Lamu-rift zone; ANFZ= Aswa-Nyangia-fault zone; AFZ = Anza-fault zone

Acknowledgment:

This study was funded through a postgraduate training scholarship by Japan International Cooperation Agency (JICA) at the Research Centre for Seismology, Volcanology and Disaster Mitigation in Nagoya University, Japan.